

Combining various projection access schemes with the algebraic reconstruction technique for low-contrast detection in computed tomography

Huaiqun Guan^{†‡}, Richard Gordon[§] and Yunping Zhu[†]

[†] Department of Radiation Oncology, St Jude Children's Research Hospital, Memphis, TN 38105, USA

[§] Departments of Radiology and Physics, University of Manitoba, Winnipeg, Manitoba, R3T 2N2, Canada

Received 4 December 1997

Abstract. We separately applied three different projection access orders (the multilevel scheme (MLS), the sequence access scheme (SAS) and the random permutation scheme (RPS)) to the algebraic reconstruction technique (ART) in an attempt to improve low-contrast object detection in computed tomography (CT). We used both simulated (from various numbers of projections of low-contrast and contrast detail phantoms) and actual data (from megavoltage portal CT) during our study. When coupled with ART, SAS and RPS led to poor low-contrast detection and required multiple iterations for convergence. In contrast, one-iteration MLS yielded the most uniform reconstructions with the highest contrast-to-noise ratios. Therefore, MLS-ART provides the highest dose efficiency of all current reconstruction techniques for imaging low-contrast objects from a small number of projections.

1. Introduction

Low-contrast detectability is strongly dose dependent, and for some situations in radiographic imaging, high-contrast resolution is not as important as the ability to provide excellent image contrast (Yaffe and Rowlands 1997). Such is the case with megavoltage portal imaging for radiation treatment verification. In portal imaging, the high-energy x-ray photons experience inherently low attenuation in tissues. In addition, attenuation of radiation by tissues in this energy range is mainly due to Compton scattering that depends on electron density but not the atomic number. The two factors combined resulted in poor differentiation between various tissues (Johns and Cunningham 1983). Further, the detective quantum efficiency (DQE) of current electronic portal imaging devices (EPIDs) is nearly two orders of magnitude lower than those of detectors for diagnostic x-ray computed tomography (CT) (Munro 1995, Boyer *et al* 1992). Overcoming these limitations of EPID for megavoltage portal CT requires developing an efficient reconstruction technique, especially one that is optimal for situations of low-contrast detectability.

In an attempt to achieve dose-efficient CT reconstructions, we previously evaluated three projection access schemes for use with the algebraic reconstruction technique (ART). We found that the multilevel scheme (MLS) (Guan and Gordon 1994) outperforms the random permutation scheme (RPS) and the sequential access scheme (SAS), the two conventionally

[‡] E-mail address: huaiqun.guan@stjude.org

used projection access orders (Guan and Gordon 1996). Further, MLS essentially makes ART a non-iterative technique, as most of the convergence occurred within the first iteration. To further address the suitability of MLS-ART for low-contrast detectability, we needed to design appropriate phantoms.

For the present study, we designed two computed-based low-contrast phantoms (see section 2). We compared the performance of MLS, SAS and RPS for ART by using the simulated projection data from these phantoms (see section 3). We then extended the study by using data from an actual portal CT (see section 4). We show that when combined with SAS and RPS, ART leads to poor low-contrast detection and requires multiple iterations to achieve convergence. In contrast, one-iteration MLS-ART produced the uniform and smooth reconstructions, which also had large contrast detectability.

2. Phantom design for simulation

We designed low-contrast (figure 1(a)) and contrast detail (figure 1(b)) phantoms (both are computer-generated mathematical phantoms), in which the outermost circle simulates bone (we used 8 bits to do the simulation and assume bone has the largest CT number of 255). The inner region simulates soft tissue (average CT number of 127), and the area beyond the circle is air (CT no = 0). Both of the phantoms have an overall diameter of 25 cm (512×512 pixels in size, 0.5 mm/sample), close to the size of an adult head. The physical details of simulation (using 8 bits) were discussed in Guan and Gordon (1996). The range of the CT number in this simulation study bears a linear relationship to that in diagnostic CT.

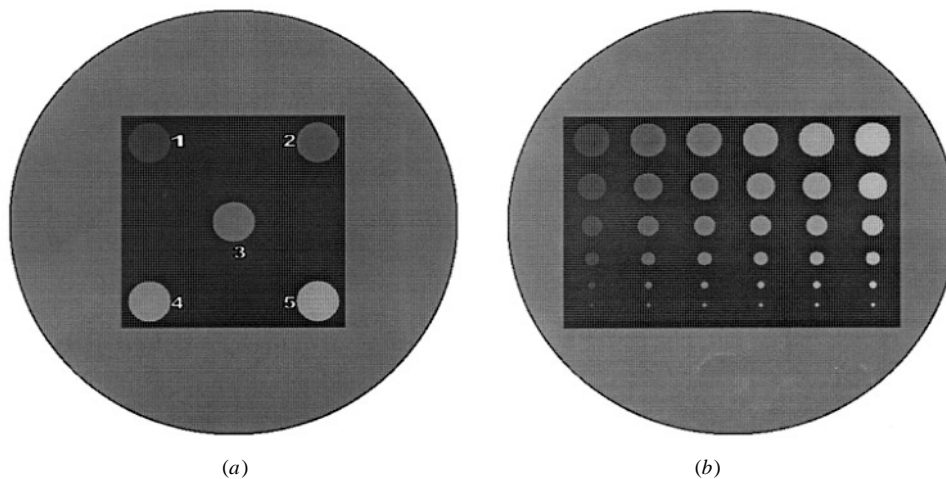


Figure 1. Low-contrast (a) and contrast detail (b) phantoms. Both are 25 cm in diameter, cover a round area of 512 pixels in diameter and contain 255 grey levels. For both phantoms, the central regions were windowed to a smaller range of grey levels (centre 124; width 12) to enhance visual contrast.

We calculate the disc's contrast using the formula

$$C = \frac{|\text{CT no 1} - \text{CT no 2}|}{|\text{CT no 1} + \text{CT no 2}|}$$

where CT no 1 is the disc's CT no and CT no 2 is the background's CT no. In the low-contrast phantom, there are five discs of 2.3 cm in diameter. We set

$|\text{CT no 1} - \text{CT no 2}|$ = the disc's index number (for example, disc 3 has a CT number of $127 - 3 = 124$). $|\text{CT no 1} + \text{CT no 2}|$ is nearly 250. Disc 1 has a contrast of $1/250 = 0.4\%$, which approximates the detection limit of x-ray CT (0.5%). The contrasts of other discs are equal to their index number multiplied by 0.4% (for example, disc 3's contrast is $3 \times 0.4\% = 1.2\%$). In order to better visualize these discs, we windowed the central part of the phantom to a CT number of 124, with the window width equal to 12.

In the contrast detail phantom (figure 1(b)), there are six rows of discs. Each row contains six discs of the same size but differing contrast. From top to bottom, the discs are 2.0, 1.6, 1.2, 0.8, 0.4 and 0.2 cm in diameter. From left to right, disc contrast increases in 0.4% increments, from 0.4% to 2.4%. Again, for enhanced visual contrast, the central part of the phantom is windowed to a CT number of 124 and a width of 12.

We calculated ray integrals along a series of angles to obtain a set of projection data for each phantom. Before reconstruction, we introduced physically realistic Poisson noise into these data by setting the photon number per ray at 1.28×10^7 (approximating that in x-ray CT using 60 keV photons). We used our published computing procedure (Guan and Gordon 1996) to do the calculations.

3. Computer simulation study

We separately compared the performance of MLS and SAS and of MLS and RPS, using the two simulated phantoms. The MLS and SAS schemes are the two extreme situations of ordering. The former reduces the geometrical correlation among projections to a minimum while the latter has the maximum correlation. The former allows multilevel multiresolution reconstructions (due to its uniform angular distribution at each level), while the latter does not allow these at all. The convergence performance of RPS is in between those of MLS and SAS.

3.1. MLS versus SAS

We used 100 projections of the low-contrast phantom to compare MLS with SAS (figure 2). After one (figure 2(a)), six (figure 2(b)), and even 12-iterations (figure 2(c)) of SAS, much of the object is poorly reconstructed, and discs having increased contrast cannot be distinguished. Although the full features are adequately reconstructed after 20 iterations (figure 2(d)), the image appears noisier than that obtained by using one-iteration MLS (figure 2(e)).

We defined the contrast-to-noise ratio (CNR)

$$\text{CNR} = \frac{|\text{CT no 1} - \text{CT no 2}|}{\sqrt{\sigma_1^2 + \sigma_2^2}}$$

to quantify the contrast of these reconstructed noise-containing discs against their noise-containing background. CT no 1 is the mean CT number within a disc, and CT no 2 is that within an equal area of the background; σ_1 and σ_2 are the two corresponding noise standard deviations. The noise in CT images is not strictly Gaussian in distribution; the noise power spectrum (NPS) has to be used to completely characterize CT noise. However, this noise is close to being Gaussian (Guan and Gordon 1998). In fact, the single measurement of the noise standard deviation (without addressing noise correlation) is frequently used for quality assurance of CT scanners. Similar definitions of CNR have previously been used for evaluating CT images (Goodenough and Weaver 1981) and, recently, for measuring radiographic/fluoroscopic image quality (Boone and Seibert 1994).

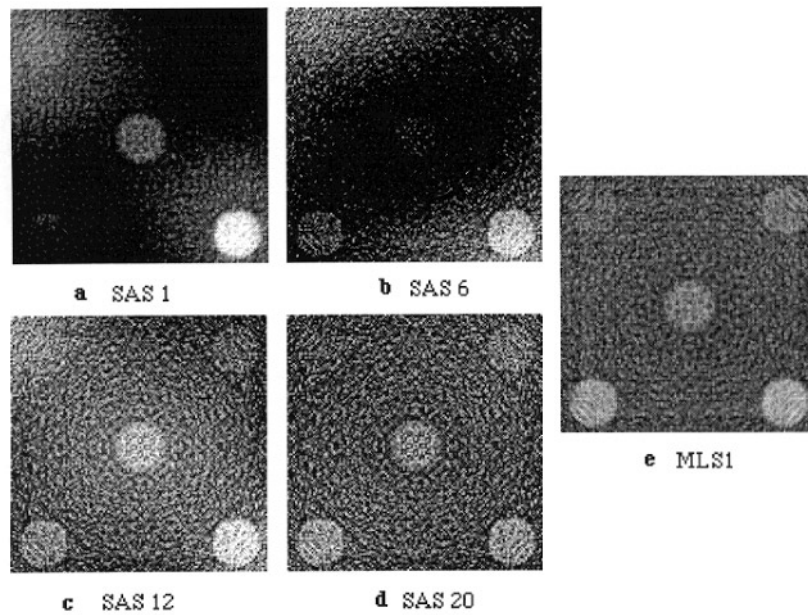


Figure 2. Images of the low-contrast phantom reconstructed by using 100 projections and one- (a), six- (b), 12- (c), 20-iteration SAS (d) or one-iteration MLS (e).

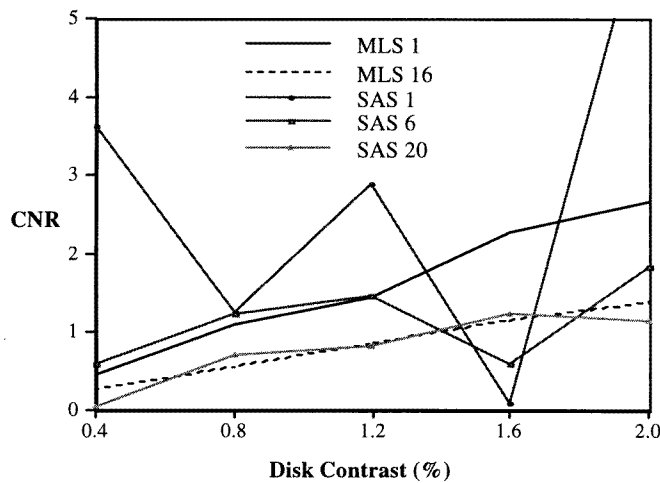


Figure 3. The contrast-to-noise ratio (CNR) from the reconstructions of the five discs in the low-contrast phantom versus their contrast values after one- or 16-iteration MLS or one-, six- or 20-iteration SAS. We used 100 projections.

For the reconstructions obtained after one- and 16-iteration MLS and one-, six- and 20-iteration SAS, we separately plotted the measured CNR values of the discs against disc contrast (figure 3). The CNR from the MLS-based reconstructions monotonically and almost linearly increased with disc contrast—the first iteration has the largest CNR. But for reconstructions based on one- and six-iteration SAS, discs with increased contrast

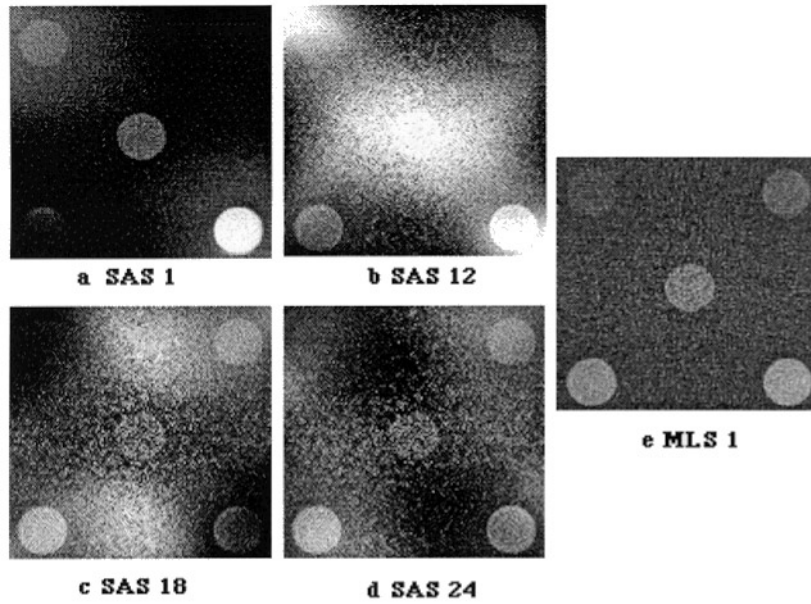


Figure 4. Images of the low-contrast phantom reconstructed from 800 projections by using one- (a), 12- (b), 18- (c) or 24-iteration SAS (d) or one-iteration MLS (e).

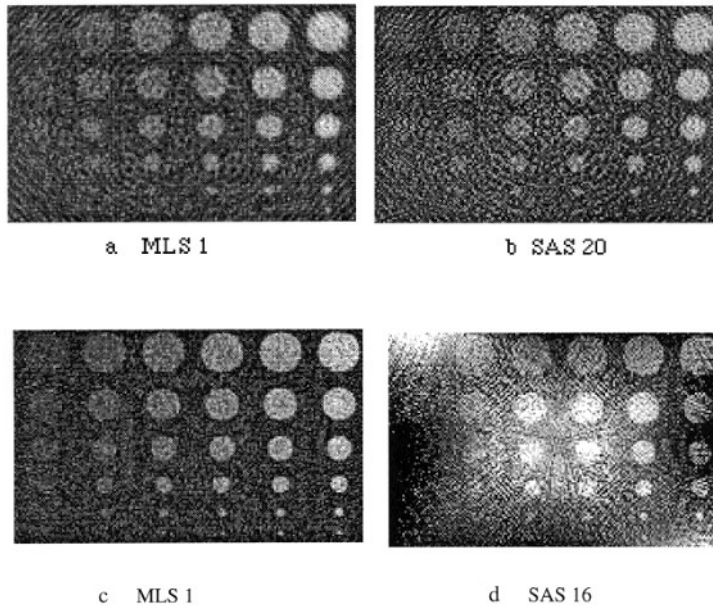


Figure 5. Images of the contrast detail phantom reconstructed by using 100 projections and one-iteration MLS (a) or 20-iteration SAS (b) or by using 400 projections and one-iteration MLS (c) or 16-iteration SAS (d).

were associated with lower CNR values, and those with less contrast had larger CNR values. Although the 20-iteration SAS converges to a reasonable curve with regard to

contrast, the associated CNR values are only half those obtained by using one-iteration MLS. The performance of SAS becomes even poorer when the number of projections is increased (for example, 800 projections in figure 4). In this case, image features are not correctly reconstructed even after 24-iteration SAS. However, one-iteration MLS produces a satisfactory reconstruction, with all five discs clearly distinguishable.

We then tested one-iteration MLS (figure 5(a)) and 20-iteration SAS (figure 5(b)) for reconstructing images from 100 projections of the contrast detail phantom. Similar to findings for the low-contrast phantom (figure 2), reconstructions based on 20-iteration SAS have more noise than those generated through one-iteration MLS. We applied one-iteration MLS (figure 5(c)) and 16-iteration SAS (figure 5(d)) to 400 projections of this phantom. In this case, although the convergence speed was faster than that for 800 projections, 16-iteration SAS was still far from yielding a uniform reconstruction.

3.2. MLS versus RPS

We then compared MLS with RPS. We found that for 200 projections, the performance of one-iteration RPS (figures 6(b) and (c)) was poorer than that of one-iteration MLS (figure 6(a)). RPS performs relatively better at 800 projections (figures 6(e) and (f)) than at 200, although the noise remained slightly higher than that for one-iteration MLS (figure 6(d)). This improvement in the performance of RPS probably occurred because two projections selected are more likely to be further apart from each other when the pool of projections is increased. With the contrast detail phantom, the reconstructions based on one-iteration MLS (figure 7(a) and (c)) and one-iteration RPS (figures 7(b) and (d)) were more similar and better when we used 800 projections than when 200 projections were used.

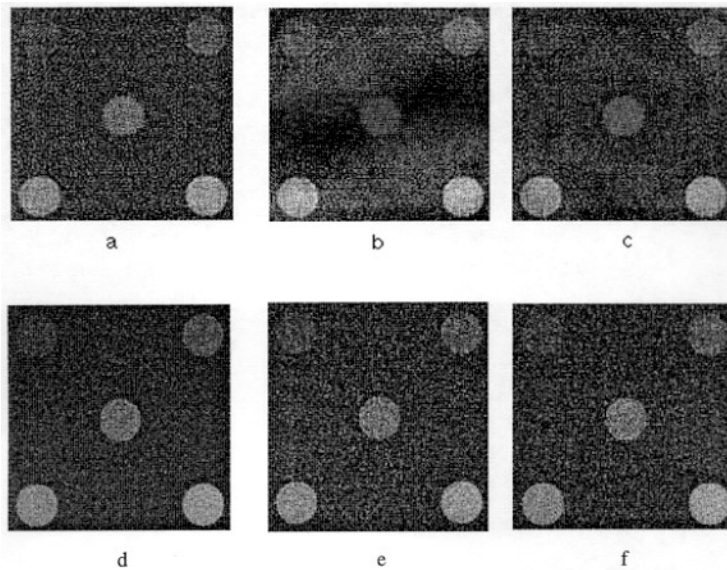


Figure 6. Images of the low-contrast phantom reconstructed from 200 projections by using one-iteration MLS (a) or one-iteration RPS (b) and (c; two random reconstructions) or from 800 projections by using one-iteration MLS (d) or one-iteration RPS (e) and (f; two random reconstructions).

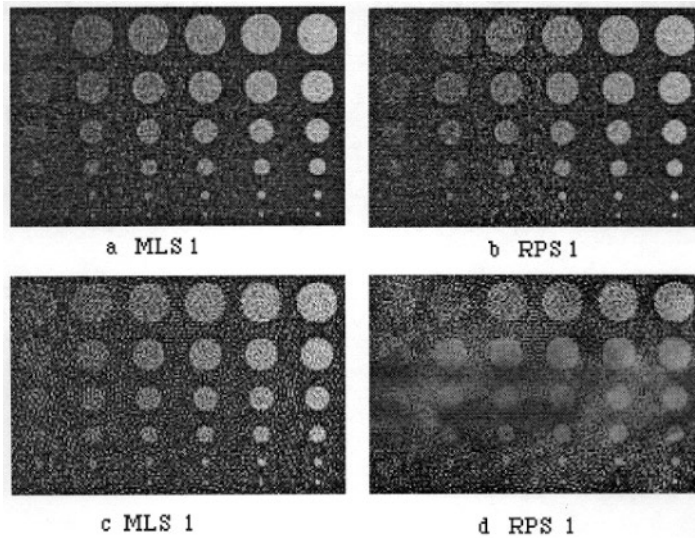


Figure 7. Images of the contrast detail phantom reconstructed from 800 projections by using one-iteration MLS (a) or one-iteration RPS (b) or from 200 projections by using one-iteration MLS (c) or one-iteration RPS (d).

4. Applying actual projection data

We then used the projection data obtained by an EPID for portal CT reconstructions. We set the EPID at its linear dynamic range as a CT detector and collimated 6 MV photons from a linear accelerator to a slit beam 1 cm wide and 25 cm long. We performed scans of various physical phantoms, including a low-contrast phantom and a Rando head phantom (see Guan and Zhu (1998) for details) using 200 total monitor units (MUs) in which we varied the number of projections and MUs per projection.

We chose to use a fan beam with a small angle (14.5°) so that the rays in each projection were nearly parallel. Therefore, we only ordered the resulting projections into the three different access schemes, not the rays inside each projection. However, for image reconstruction, we developed a fan-beam algorithm for ART to accommodate the specific third-generation CT geometry that we used. Because we had to manually rotate the linear accelerator gantry for data acquisition, we collected only a limited number of projections.

Here we demonstrate the CT images of a low-contrast phantom using a total of 50 fan beam projections covering $180^\circ + 14.5^\circ$. The phantom is 25 cm in diameter. The discs inside are made of Lucite and embedded in water. The diameters of the three largest disc sets are 1.3, 1.0 and 0.8 cm respectively. We delivered 4 MU of radiation at each gantry angle (total 200 MU). We then reconstructed the images to a 256×256 matrix by using one-iteration MLS (figure 8(a)), one-iteration RPS (figures 8(b) and (c), two different orders), one-iteration SAS (figure 8(d)), and three-iteration SAS (figure 8(e)). The performance of all three schemes was similar to what it had been for smaller number of projections (100 or 200) from simulated data.

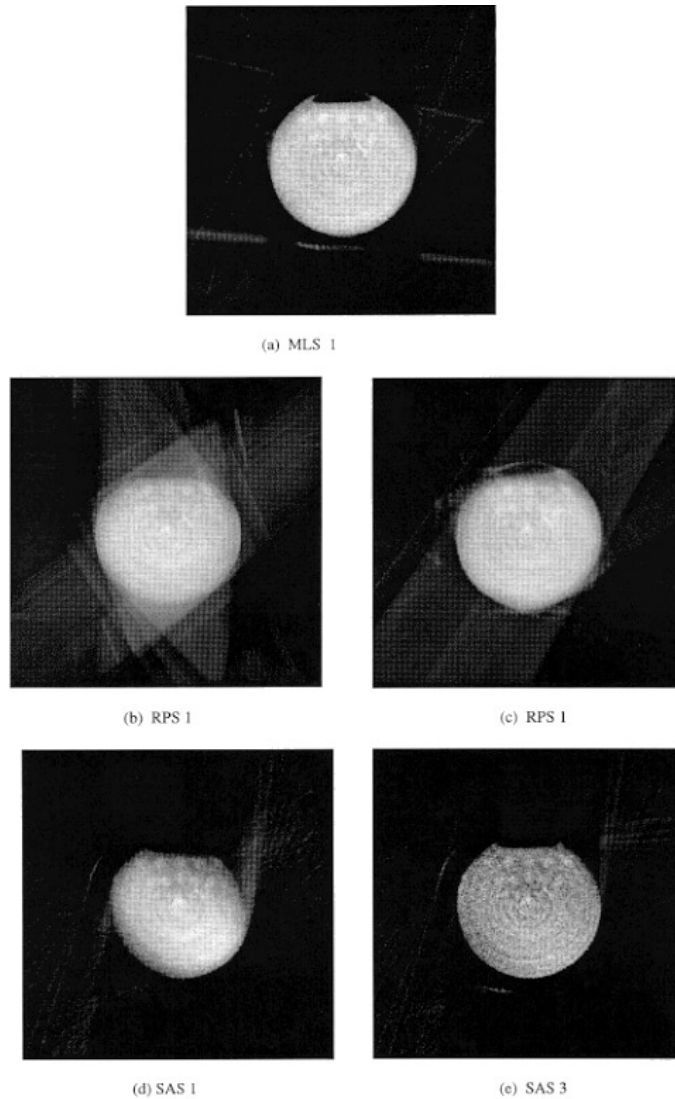


Figure 8. A low-contrast CT phantom scanned by using an electronic portal imaging device; a total of 50 fan projections covering $180^\circ + 14.5^\circ$ (fan angle) were acquired. The scanning beam was a $25\text{ cm} \times 1\text{ cm}$ slit. At each gantry angle, 4 MU radiation were delivered (total 200 MU). Each image is 256×256 pixels in size, and each pixel covers an area of $\sim 2\text{ mm} \times 2\text{ mm}$. The images were reconstructed by using one-iteration MLS (a), one-iteration RPS (b) and (c); two random projections), one-iteration SAS (d), or three-iteration SAS (e).

5. Discussion and conclusion

In the present paper we show that of three projection access schemes, MLS provides the maximum projection orthogonality during reconstruction and the most spatial uniformity.

It is worth noting that SAS converges faster for a smaller matrix than it does for a larger one under the same sampling conditions. A four-iteration SAS was sufficient for a 64×64 matrix using 100 projections (Guan and Gordon 1996), but it was far from yielding a

uniform reconstruction for a 512×512 matrix with 800 projections (figure 4), even though the sampling criterion was satisfied in both cases. The key disadvantage of SAS is that it cannot reconstruct objects uniformly and symmetrically; features are severely distorted (twisted) during early iterations. Using SAS to reconstruct a low-contrast object from a large matrix and a large number of projections is very computing intensive. Even when a uniform reconstruction is obtained after the many necessary iterations, its low-contrast detectibility fails to match that from a one-iteration MLS. We also noticed that the performance of RPS varies with image size and number of projections. Its convergence is relatively slow not only for a small projection number but also for a small matrix, as figure 8 demonstrates. Although superior to SAS, RPS is not a reliable ordering scheme.

We demonstrated that when projection data are limited, MLS-ART outperforms the conventional CBP technique for low-contrast detection (Guan and Gordon 1998). In the present study, we showed that MLS also improves the detectibility of ART itself. Therefore, MLS-ART provides the highest dose efficiency of all current reconstruction techniques for imaging low-contrast objects from a small number of projections.

Acknowledgments

The authors thank Inhwan J Yeo, Waleed Gaber, Yonas Yohannes and Xunqing Jiang for assisting with the data acquisition during portal CT. We acknowledge the therapeutic technologists of Radiation Oncology for their help with the linear accelerator. We thank Amy L B Frazier for editing the manuscript. We also thank the anonymous referees for their valuable comments on the original manuscript and their suggestions on improving it. This work is supported in part by grant R29 CA65606 from the National Cancer Institute, by the Whitaker Foundation, and by the American Lebanese and Syrian Associated Charities (ALSAC).

References

- Boone J M and Seibert J A 1994 A comparison of mono- and poly-energetic x-ray beam performance for radiographic and fluoroscopic imaging *Med. Phys.* **21** 1853–63
- Boyer A L, Antonuk L, Fenster A, Van Herk M, Meertens H, Munro P, Reinstein L E and Wong J 1992 A review of electronic portal imaging devices (EPIDs) *Med. Phys.* **19** 1–16
- Goodenough D J and Weaver K E 1981 Introduction to computed tomography *Computed Tomography in Radiation Therapy* ed C C Ling, C C Rogers and R J Morton (New York: Raven Press) pp 121–7
- Guan H and Gordon R 1994 A projection access order for speedy convergence of ART: A multilevel scheme for computed tomography *Phys. Med. Biol.* **39** 2005–22
- 1996 Computed tomography using ART with different projection access schemes: a comparison study under practical situations *Phys. Med. Biol.* **41** 1727–43
- 1998 Computed tomography using multilevel scheme algebraic reconstruction technique (MLS-ART) compared to the convolution backprojection (CBP) method for low contrast detection *Phys. Med. Biol.* submitted
- Guan H and Zhu Y 1998 Megavoltage portal CT reconstruction using a novel MLS-ART technique and a fluorescent screen/CCD based EPID *Phys. Med. Biol.* submitted
- Johns H E and Cunningham J R 1983 *The Physics of Radiology* 4th edn (Springfield, IL: Thomas)
- Munro P 1995 Portal imaging technology: past, present and future *Semin. Radiat. Oncol.* **5** 115–33
- Yaffe M J and Rowlands J A 1997 X-ray detectors for digital radiography *Phys. Med. Biol.* **42** 1–39